Modification of $(Zn_{1+x}Ge)(N_2O_x)$ Solid Solution as a Visible Light Driven Photocatalyst for Overall Water Splitting

Yungi Lee,[†] Kentaro Teramura,[†] Michikazu Hara,[‡] and Kazunari Domen*[,†,§]

Department of Chemical System Engineering, The University of Tokyo, 7-3-1 Hongo, Bunkyo-ku, Tokyo 113-8656, Japan, Materials and Structures Lab, Tokyo Institute of Technology, 4259 Nagatsuta, Midori-ku, Yokohama 226-8503, Japan, and Solution-Oriented Research for Science and Technology, Japan Science and Technology Co., 2-1-13 Higashiueno, Taito-ku, Tokyo 110-0015, Japan

Received December 15, 2006. Revised Manuscript Received February 14, 2007

Zinc germanium oxynitride, a solid solution between ZnO and $ZnGeN_2$, is prepared by reaction of GeO_2 and ZnO under a NH_3 flow (20 mL min^{-1}) at 1123 K. Samples nitrided for 5−15 h under these conditions exhibit a single phase of wurtzitic $(Zn_{1+x}Ge)(N_2O_x)$, and are responsive to visible light with a band gap of ca. 2.7−2.8 eV. The band gap decreases slightly with increasing nitridation time, that is, with increasing zinc content, attributable to p−d repulsion between Zn3d and N2p + O2p electrons in the upper valance band, which raises the top of the valance band. Nitridation for 15 h afforded $(Zn_{1+x}Ge)(N_2O_x)$ with the highest photocatalytic activity for overall water splitting. The optimized catalyst has high crystallinity due to complete reaction of the starting materials, without volatilization of zinc from the product under prolonged reduction. A range of cocatalysts is also examined, and $Rh_{2-x}Cr_xO_3$ is identified as the most effective cocatalyst for $(Zn_{1+x}Ge)(N_2O_x)$, which greatly causes an increase in the activity for hydrogen evolution. Modification of the optimized $(Zn_{1.44}Ge)(N_{2.08}O_{0.38})$ sample by loading with $Rh_{2-x}Cr_xO_3$ (3.0 wt % Rh, 0.2 wt % Cr) results in an effective photocatalyst for overall water decomposition with a quantum efficiency of ca. 0.20% at 420 nm.

Introduction

Photocatalysts for overall water splitting have been studied extensively for the purpose of solar energy conversion of hydrogen as an energy carrier. To improve the utilization of sunlight, substantial effort has been devoted to the sensitization of photocatalysts for the abundant visible region. Some of the present authors recently reported that solid solutions of ZnO and other wide band gap semiconductors such as GaN or $ZnGeN_2$ exhibit band gaps smaller than 3.0 eV and thus activity at visible wavelengths. These solid solutions, $(Ga_{1-x}Zn_x)(N_{1-x}O_x)$[1−3] and $(Zn_{1+x}Ge)(N_2O_x)$,[4] have smaller band gaps than the constituent semiconductors (ZnO, 3.2 eV;[5] GaN, 3.4 eV;[6] $ZnGeN_2$, 3.3 eV[7]) and, when loaded with an appropriate cocatalyst, achieve overall water splitting under visible light irradiation.

In the previous paper, $(Zn_{1+x}Ge)(N_2O_x)$ powder was confirmed to be a solid solution between ZnO and $ZnGeN_2$, and the material was demonstrated to exhibit photocatalytic activity for overall water splitting under both ultraviolet (UV) and visible irradiation after surface modification with RuO_2. However, the detailed physical properties and optimum preparation condition for $(Zn_{1+x}Ge)(N_2O_x)$ have yet to be determined. In the present study, the optimum preparation conditions for this photocatalyst are identified by systematic investigation of the relationship between physical properties and photocatalytic activity. Suitable cocatalysts are also investigated, leading to a highly efficient $(Zn_{1+x}Ge)(N_2O_x)$ photocatalyst.

Experimental Section

Preparation of $(Zn_{1+x}Ge)(N_2O_x)$ solid solution. $(Zn_{1+x}Ge)(N_2O_x)$ was prepared by heating a mixture of GeO_2 (Kanto Chemicals; 99.99%) and ZnO (Kanto Chemicals; 99%) powders (ca. 2.0 g) under flowing NH_3 at high temperature. Solid solutions with a Zn/Ge molar ratio of 5 were subsequently nitrided at 1123 K under NH_3 flow (20 mL min^{-1}) for 5−20 h. Excess ZnO was provided to counter volatilization of zinc due to reduction of ZnO upon exposure to the reductive atmosphere of nitridation. After nitridation, the sample was cooled to room temperature under a NH_3 flow. Prior to characterization and photocatalytic reaction, samples containing residues were treated in HNO_3 solution to ensure complete residue removal.

Characterization. Structures were characterized by X-ray diffractometry (XRD; RINT 2100, Rigaku) using Cu K_α radiation at 40 kV and 40 mA. The XRD patterns were collected at 2θ angles of 10−70° at a scan rate of 1° min^{-1}. The surface morphologies and average particle sizes of products were observed by field-

* To whom correspondence should be addressed. E-mail: domen@chemsys.t.u-tokyo.ac.jp. Phone: 81-3-5841-1148. Fax: +81-3-5841-8838.
[†] The University of Tokyo.
[‡] Tokyo Institute of Technology.
[§] Japan Science and Technology Co.

(1) Maeda, K.; Takata, T.; Hara, M.; Saito, N.; Inoue, Y.; Kobayashi, H.; Domen, K. *J. Am. Chem. Soc.* **2005**, *127*, 8286−8287.
(2) Maeda, K.; Teramura, K.,; Takata, T.; Hara, M.; Saito, N.; Toda, K.; Inoue, Y.; Kobayashi, H.; Domen, K. *J. Phys. Chem. B* **2005**, *109*, 20504−20510.
(3) Maeda, K.; Teramura, K.; Takata, T.; Lu, D.; Saito, N.; Inoue, Y.; Domen, K. *Nature (London)* **2006**, *440*, 295.
(4) Lee, Y.; Tararshima, H.; Shimodaira, Y.; Teramura, K.; Hara, M.; Kobayashi, H.; Domen, K.; Yashima, M. *J. Phys. Chem. B* **2007**, in press.
(5) Kocha, S. S.; Peterson, M. W.; Arent, D. J.; Redwing, J. M.; Tischler, M. A.; Turner, J. A. *J. Electrochem. Soc.* **1995**, *142*, L238−L240.
(6) Nakamura, S. *Science* **1998**, *281*, 956−961.
(7) Larson, W. L.; Maruska, H. P.; Stevenson, D. A. *J. Electrochem. Soc.: Solid State Sci. Technol.* **1974**, *121*, 1673.

10.1021/cm062980d CCC: $37.00
Published on Web 03/23/2007

emission scanning electron microscopy (SEM; S-4700, Hitachi). The chemical composition was determined by inductively coupled plasma optical emission spectroscopy (ICP-OES; Iris Advantage DuO, Thermo Elemental Co.) and a TC436 oxygen and nitrogen determinator (LECO Co.). The surface states of the (Zn$_{1+x}$Ge)-(N$_2$O$_x$) solid solutions were examined by X-ray photoelectron spectroscopy (XPS; ESCA 3200, Shimadzu). All binding energies were corrected using the binding energy of Au 4f$_{7/2}$ (83.8 eV). UV−visible diffuse reflectance spectrometry (DRS; V-560, Jasco) was performed in reference to $BaSO_4$ powder.

Modification of (Zn$_{1+x}$Ge)(N$_2$O$_x$). RuO_2, Cr_2O_3, Fe_2O_3, Co_3O_4, NiO, CuO, ZnO, Rh_2O_3, and $Rh_{2-x}Cr_xO_3$ were examined as particulate cocatalysts. The cocatalyst was loaded in each case onto the as-prepared (Zn$_{1+x}$Ge)(N$_2$O$_x$) powder. RuO_2 was loaded by an impregnation method as described in the previous paper.[4] Cr_2O_3, Rh_2O_3, and $Rh_{2-x}Cr_xO_3$ were loaded by impregnation from Cr(NO$_3$)$_3$·9H$_2$O (Kanto Chemicals; >98.0%) and/or Na$_3$RhCl$_6$·2H$_2$O (Kanto Chemicals; >98.0%). Similarly, Fe(NO$_3$)$_3$·9H$_2$O (Kanto Chemicals; >99.9%), Co(NO$_3$)$_2$·6H$_2$O (Kanto Chemicals; >98.0%), Ni(NO$_3$)$_2$·6H$_2$O (Kanto Chemicals; >98.0%), Cu(NO$_3$)$_3$·3H$_2$O (Wako Chemicals; >99.0%), and Zn(NO$_3$)$_2$·H$_2$O (Kanto Chemicals; >99.0%) were used for impregnation of Fe_2O_3, Co_3O_4, NiO, CuO, and ZnO. The resultant mixture was calcined in air at 573−623 K for 1 h prior to reaction and then oxidized as a cocatalyst. Pt was loaded as a cocatalyst for photoreduction of H^+ to H_2 by in situ photodeposition using H_2PtCl_6 in 10 vol % methanol aqueous solution.

Photocatalytic Activity. Reactions were carried out in a Pyrex inner irradiation-type reaction vessel connected to a glass closed gas circulation system. The reaction was performed in distilled water containing 0.20 g of the cocatalyst-loaded sample. The reactant solution was initially evacuated several times to remove air completely and then irradiated under a 450 W high-pressure Hg lamp (λ > 300 nm). The photocatalytic activity under visible light irradiation (λ > 420 nm), photoreduction and photooxidation reactions, and apparent quantum efficiency were measured with the use of a Pyrex top irradiation-type reaction vessel and a 300 W xenon lamp with a cutoff filter or band-pass filter. Photoreduction of H^+ to H_2 was examined using an aqueous solution (200 mL) containing 0.10 g of the sample and 20 mL of methanol. Photooxidation of water to O_2 was performed using an aqueous $AgNO_3$ solution (0.01 mol dm^{-3}, 200 mL).

The apparent quantum efficiency (Φ) was estimated by the following equation.

$$\Phi(\%) = \frac{\text{no. of reacted electrons}}{\text{no. of incident photons}} \times 100 = \frac{\text{no. of evolved } H_2 \text{ molecules} \times 2}{\text{no. of incident photons}} \times 100$$

Here, Φ is the apparent quantum efficiency, where it is assumed that all incident photons are absorbed by the reaction system. The number of incident photons 4.48×10^{20} photon h^{-1} at 420 nm was measured using a Si photodiode. The evolved gases were analyzed by gas chromatography with a thermal conductivity detector (GC-8A, Shimadzu; Ar carrier gas).

Results and Discussion

XRD Patterns, Elementary Analyses, and SEM Images. Figure 1 shows the XRD patterns of the samples prepared at 1123 K under a NH_3 flow at 20 mL min^{-1} for various nitridation times. ZnO and $ZnGeN_2$ data are also shown for comparison. Nitridation for 5−10 h produced the wurtzite phase of (Zn$_{1+x}$Ge)(N$_2$O$_x$) with a ZnO phase as a residue,

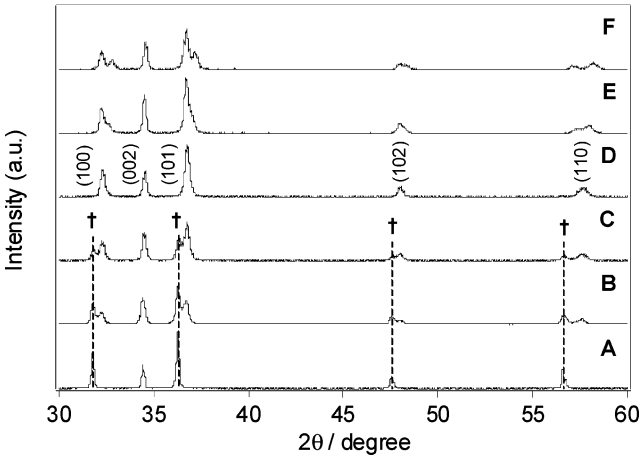

Figure 1. XRD patterns of (A) ZnO and (B−E) (Zn$_{1+x}$Ge)(N$_2$O$_x$) nitrided at 1123 K under NH_3 flow of 20 mL min^{-1} for (B) 5, (C) 10, (D) 15, and (E) 20 h, and (F) $ZnGeN_2$. † = ZnO phase.

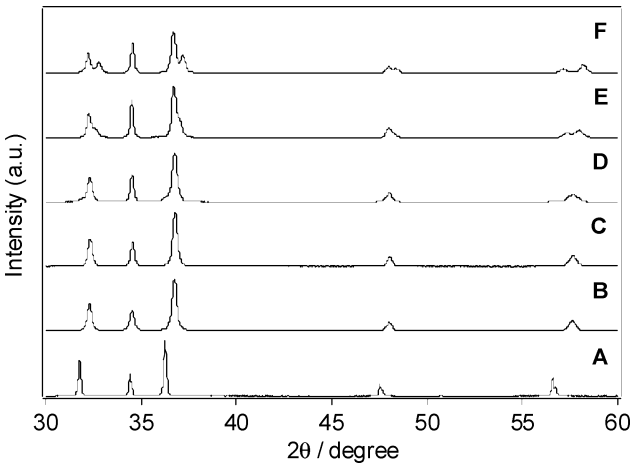

Figure 2. XRD patterns of (A) ZnO, (B−E) HNO_3-treated (Zn$_{1+x}$Ge)-(N$_2$O$_x$) samples nitrided for (B) 5, (C) 10, (D) 15, and (E) 20 h, and (F) $ZnGeN_2$.

although the intensity of the relevant XRD peak for ZnO was quite low. As the nitridation time was increased from 5 to 15 h, the ZnO phase became less apparent, and the (Zn$_{1+x}$-Ge)(N$_2$O$_x$) phase became more prominent. Nitridation for 15 h resulted in a sample with only a single phase in the diffraction pattern, indicating the sole presence of the wurtzite structure without other impurity phases or residues. However, nitridation for longer than 15 h caused the peaks indexed to (100), (101), and (110) to split. The sample nitrided for 20 h (Figure 1E) exhibits an XRD pattern similar to that of $ZnGeN_2$ (Figure 1F), suggesting that the change in the XRD pattern is attributable to symmetry change from wurtzite to an orthorhombic structure due to a decrease of zinc content as a result of volatilization of zinc to zinc vapor during the extended nitridation process.

Figure 2 shows the XRD patterns of the samples after treatment with HNO_3 solution to remove residual ZnO. After HNO_3 treatment, the samples nitrided for 5−10 h exhibit a single phase corresponding to the (Zn$_{1+x}$Ge)(N$_2$O$_x$) solid solution. (lines B and C of Figure 2). The XRD measurements revealed that a single phase of (Zn$_{1+x}$Ge)(N$_2$O$_x$) with a wurtzite structure was obtained by nitridation for 5−15 h. The lattice parameters of these samples vary from 3.2022 to 3.2031 Å (*a*-axis length) and 5.1985 to 5.2026 Å (*c*-axis

Table 1. Elemental Analyses of $(Zn_{1+x}Ge)(N_2O_x)$ Samples Prepared with Various Nitridation Times

	element content (at %)				
t (h)	Ge	Zn	N	O	chemical composition
5	22.5	28.0	39.2	10.3	$(Zn_{1.25}Ge)(N_{1.78}O_{0.46})$
10	22.2	28.0	40.7	9.1	$(Zn_{1.26}Ge)(N_{1.83}O_{0.41})$
15	20.4	29.3	42.5	7.8	$(Zn_{1.44}Ge)(N_{2.08}O_{0.38})$

length), which are smaller than the values for ZnO ($a = 3.253$ Å, $c = 5.213$ Å).[8] This result is reasonable given the smaller ionic radius of Ge^{4+} (0.39 Å) compared to Zn^{2+} (0.60 Å). The elemental analyses shown in Table 1 reveal that the nitrogen content in the products increased with nitridation time, whereas the oxygen content decreased. In contrast, the zinc content increased only slightly, from 28 at % to 29.3 at %, as the nitridation time was increased from 5 to 15 h. No successive shift of XRD peaks was observed with nitridation time, consistent with the absence of substantial change in zinc content.

The XRD measurements indicate that the solid solution phase forms in the early stage of nitridation, and is present after just 5 h of nitridation. Further reaction between $(Zn_{1+x}Ge)(N_2O_x)$ and ZnO then proceeds until the starting material (ZnO) is completely consumed, which occurs within 15 h. Further nitridation results in the volatilization of zinc in the $(Zn_{1+x}Ge)(N_2O_x)$ solid solution, resulting in a change in symmetry from wurtzite to an orthorhombic structure.

Figure 3 shows SEM images of the prepared samples, along with ZnO and $ZnGeN_2$ data for comparison. The 5 h nitrided sample (Figure 3A) exhibits irregularly shaped particles with rough surfaces and sizes of 100−500 nm. For samples nitrided for 5−15 h, the average particle size decreased and became more uniform. The 15 h nitrided sample displays regularly shaped particles with smooth surfaces and an average particle size of ca. 200 nm. However, nitridation for longer than 15 h cause the grains to become large and irregular again, probably due to crystal growth between primary particles.

Surface Analysis of $(Zn_{1+x}Ge)(N_2O_x)$. The surface composition of the samples was investigated by XPS and Auger measurements. The narrow-scan XPS spectra of the Ge3d, N1s, and O1s peaks are shown in Figure 4, along with ZnO and $ZnGeN_2$ data for comparison. The atomic ratios of Ge calculated from the areas of XPS spectra are shown in Table 2. The Ge3d peaks in the $(Zn_{1+x}Ge)(N_2O_x)$ powders shifted to lower binding energy from 31.1 to 30.8 eV as the nitridation time was increased from 5 to 15 h. The Ge3d peak for the 20 h nitrided sample appeared at 30.9 eV, which is co-incident with the position for $ZnGeN_2$. All Ge3d peaks in the $(Zn_{1+x}Ge)(N_2O_x)$ powders were located between those of metallic Ge (29.0 eV)[9] and GeO_2 (32.1 eV).[10] The difference in Ge3d peak position among Ge, GeO_2, and the $(Zn_{1+x}Ge)(N_2O_x)$ powders is due to the difference in bond polarity among Ge−Ge, Ge−O, and Ge−N bonds. The shift of the Ge3d peak corresponds to a decrease in oxygen and increase in nitrogen with increasing nitridation time. The N1s peaks for $ZnGeN_2$ and $(Zn_{1+x}Ge)(N_2O_x)$ powders were observed at 396.9−397.0 eV, independent of nitridation time. These N1s peak positions differ from that for Zn_3N_2 (395.8 eV), suggesting that the chemical environment around Zn in $ZnGeN_2$ and the $(Zn_{1+x}Ge)(N_2O_x)$ powders is different from that in Zn_3N_2.[11,12] The O1s peaks were observed at 530.4−530.6 and 531.4−531.8 eV, representing lattice oxygen and surface OH groups in the prepared $(Zn_{1+x}Ge)(N_2O_x)$ powders, respectively. No shift was observed for the O1s peak with increasing nitridation time. The existence of lattice oxygen in the $(Zn_{1+x}Ge)(N_2O_x)$ powders, which was very minor on the surface of the $ZnGeN_2$ powder, indicates that oxygen in the $(Zn_{1+x}Ge)(N_2O_x)$ powders formed bonds with Zn and Ge, even in the 20 h nitrided powder. Figure 5 shows the narrow-scan XPS spectra for $Zn2p_{3/2}$ and the Auger spectra for $ZnL_3M_{4,5}M_{4,5}$ in ZnO, $ZnGeN_2$, and the prepared $(Zn_{1+x}Ge)(N_2O_x)$ powders. The $Zn2p_{3/2}$ peak of each $(Zn_{1+x}Ge)(N_2O_x)$ powder appeared at 1021.8−1022.0 eV, which is almost co-incident with the value for Zn (1021.7 eV),[11] $ZnGeN_2$ (1022.0 eV), Zn_3N_2 (1021.9−1022.0 eV),[12,13] and ZnO (1022.3 eV), indicating no significant chemical shift of the $Zn2p_{3/2}$ peak despite the dissimilar chemical bonds with Zn. This lack of chemical shift can be attributed to the weaker sensitivity of the $Zn2p_{3/2}$ peak toward the chemical environment compared to the Ge3d peak.[13] The $ZnL_3M_{4,5}M_{4,5}$ Auger lines for ZnO, $ZnGeN_2$, and the prepared $(Zn_{1+x}Ge)(N_2O_x)$ powders, demonstrating high sensitivity to the chemical environment,[11,14,15] display two peaks, attributable to L−S coupling.[16] No peak separation in $ZnL_3M_{4,5}M_{4,5}$ Auger lines was observed in any of the samples, suggesting that all Zn exists in the same chemical environment in the present samples. The main Auger peaks for the $(Zn_{1+x}Ge)(N_2O_x)$ powders appeared in the range 989.0−989.2 eV, the kinetic energies of which are positioned between that for ZnO (988.1 eV) and that for $ZnGeN_2$ (989.9 eV). The modified Auger parameters for ZnO, $ZnGeN_2$, and $(Zn_{1+x}Ge)(N_2O_x)$ powders were calculated by adding the energies for the $Zn2p_{3/2}$ and $ZnL_3M_{4,5}M_{4,5}$ Auger peaks of each compound. The modified Auger parameters for the prepared $(Zn_{1+x}Ge)(N_2O_x)$ powders shifted from 2011.0 to 2011.5 eV with nitridation time, corresponding to a decrease in oxygen content and increase in nitrogen content. Auger parameters in the present samples shifted successively to higher values with increasing nitridation time and were located between the references of ZnO (2010.4 eV) and $ZnGeN_2$ (2011.9 eV), indicating that the difference in chemical states of Zn in each compound is associated with the polarity of the Zn−O and Zn−N bonds. The surficial zinc on the prepared $(Zn_{1+x}Ge)(N_2O_x)$ powders shown in Table 2 increased with nitridation time from 5 to 15 h, which is the same tendency as that seen for the bulk (Table 1). In

(8) Schulz, H.; Thiemann, K. H. *Solid State Commun.* **1979**, *32*, 783.
(9) Ueno, T. Jpn *J. Appl. Phys.* **1983**, *22*, 1349.
(10) Hollinger, G.; Kumurdjian, P.; Mackowski, J. M.; Pertosa, P.; Porte, L.; Duc, T. M. *J. Electron Spectrosc. Relat. Phenom.* **1974**, *5*, 237.
(11) Wagner, C. D.; Gale, L. H.; Raymond, R. H. *Anal. Chem.* **1979**, *51*, 466.
(12) Futsuhara, M.; Yoshioka, K.; Takai, O. *Thin Solid Films* **1998**, *322*, 274.
(13) Zong, F.; Ma, H.; Xue, C.; Zhuang, H.; Zhang, X.; Xiao, H.; Ma, J.; Ji, F. *Solid State Commun.* **2004**, *132*, 521.
(14) Briggs, D., Ed. *Handbook of X-ray and Ultraviolet Photoelectron Spectroscopy*; Heyden: London, 1977; pp 390−391.
(15) Schön, G. *J. Electron Spectrosc.* **1973**, 2, 75.
(16) Yin, L.; Tsang, T.; Adler, I.; Yellin, E. *J. Appl. Phys.* **1972**, *43*, 3464.

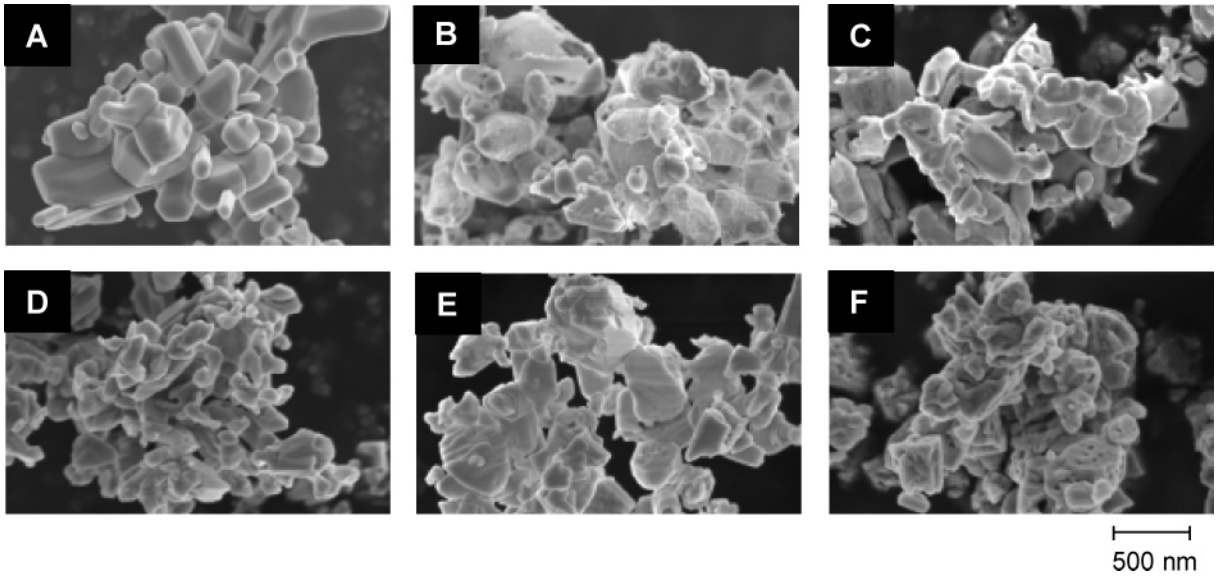

Figure 3. SEM images of (A) ZnO, (B−E) (Zn$_{1+x}$Ge)(N$_2$O$_x$) samples nitrided for (B) 5, (C) 10, (D) 15, and (E) 20 h, and (F) ZnGeN$_2$.

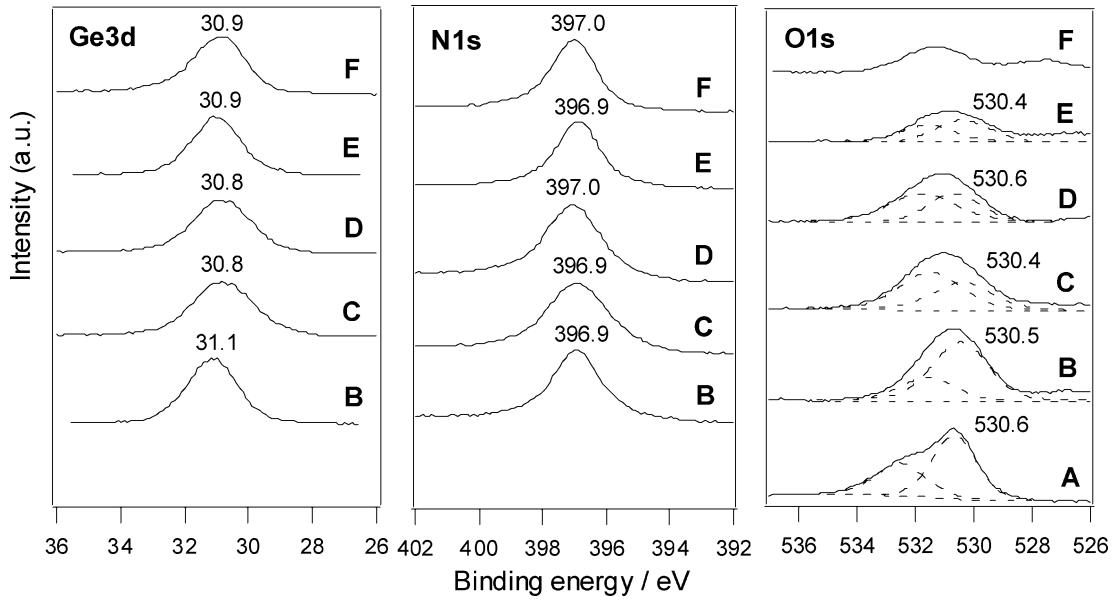

Figure 4. XPS spectra of (A) ZnO, (B−E) (Zn$_{1+x}$Ge)(N$_2$O$_x$) samples nitrided for (B) 5, (C) 10, (D) 15, and (E) 20 h, and (F) ZnGeN$_2$.

Table 2. Atomic Ratio of Zn, N, and O to Ge on Surface of (Zn$_{1+x}$Ge)(N$_2$O$_x$) Nitrided for for Various Nitridation Times

	atomic ratio[a]		
nitridation time (h)	Zn/Ge	N/Ge	O/Ge
5	1.3	1.8	0.8
10	1.5	2.0	0.6
15	1.5	2.0	0.4
20	1.0	1.9	0.3

[a] Standard error: ±0.1.

the range of nitridation time from 5 to 15 h, the zinc concentration on the surface was higher than that in the bulk, indicating that the amount of zinc supplied from ZnO to the product was larger than that volatilized from the surface during the nitridation process. However, nitridation for longer than 15 h caused the surface to become depleted in zinc (Zn/Ge = 1.0) due to volatilization of zinc from the surface without additional zinc supply.

UV−Visible DR spectra of (Zn$_{1+x}$Ge)(N$_2$O$_x$) Powders. Figure 6 shows the UV−vis DR spectra for the prepared samples along with ZnO and ZnGeN$_2$ data for comparison. ZnO is a wide band gap material with a band gap of 3.2 eV (Figure 6A). The band gap of ZnGeN$_2$ is estimated to be 3.3 eV from the edge of absorption in the UV region (Figure 6B). Although ZnO and ZnGeN$_2$ are wide band gap materials that respond only to UV light, the prepared solid solutions exhibit absorption at wavelengths longer than 400 nm. As nitridation time increases from 5 to 15 h, the absorption edge of each sample shifts slightly to longer wavelengths, suggesting a narrowing of the band gap to roughly 2.7−2.8 eV, as estimated on the basis of the onset of the UV−vis. DR spectra. After 20 h nitridation, two absorption bands appear in the UV−vis DR spectrum (Figure 6E), similar to those seen for ZnGeN$_2$. The main absorption for the 20 h nitrided sample still appears in the visible region, although the absorption edge is shifted to slightly shorter wavelengths than for the 15 h sample. The other absorption band seen in the spectrum is a broad absorption extending into the visible region (<500 nm) and is attributable to defects produced

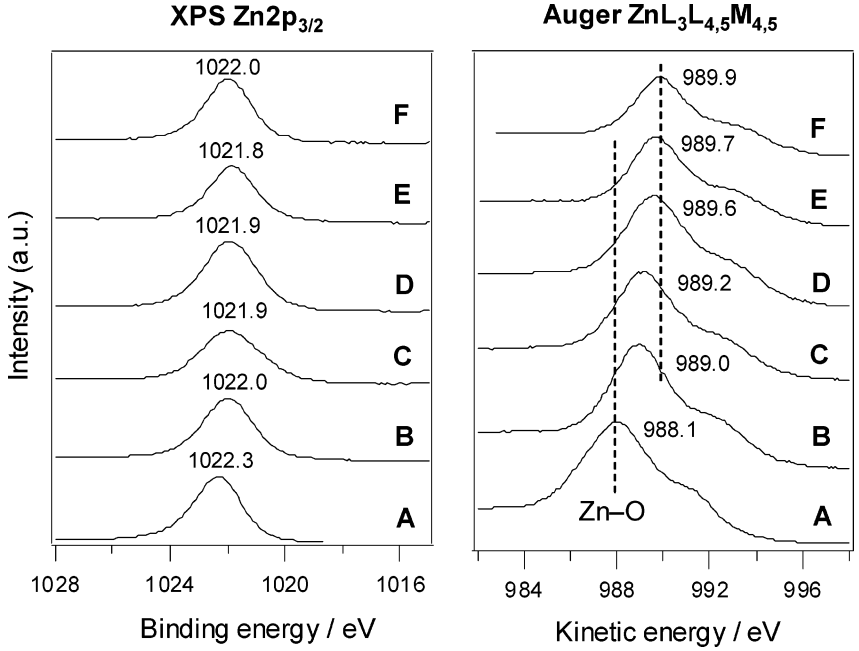

Figure 5. XPS spectra of $Zn2p_{3/2}$ and Auger spectra of $ZnL_3M_{4,5}M_{4,5}$ for (A) ZnO, (B−E) $(Zn_{1+x}Ge)(N_2O_x)$ samples nitrided for (B) 5, (C) 10, (D) 15, and (E) 20 h, and (F) $ZnGeN_2$.

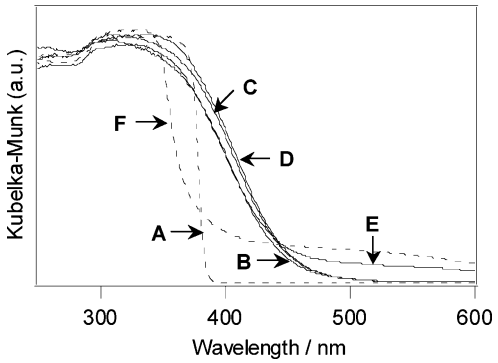

Figure 6. UV−visible DRS traces for (A) ZnO, (B−E) $(Zn_{1+x}Ge)(N_2O_x)$ samples nitrided for (B) 5, (C) 10, (D) 15, and (E) 20 h, and (F) $ZnGeN_2$.

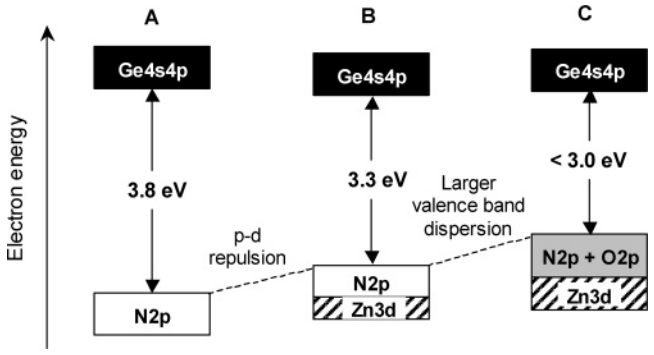

Figure 7. Band structures of (A) Ge_3N_4, (B) $ZnGeN_2$, and (C) $(Zn_{1+x}Ge)(N_2O_x)$.

during the extended nitridation process under a reductive atmosphere.

The simplified band structures of Ge_3N_4, $ZnGeN_2$ and $(Zn_{1+x}Ge)(N_2O_x)$, determined by DFT calculations,[4] are shown in Figure 7. The band gaps of the compounds decrease in the order Ge_3N_4 (3.8 eV) > $ZnGeN_2$ (3.3 eV) > $(Zn_{1+x}Ge)(N_2O_x)$ (2.7−2.8 eV). In comparison to the band gap of Ge_3N_4 (Figure 7A), the presence of Zn3d and N2p (or +O2p) electrons in the upper valence band of $ZnGeN_2$ (Figure 7B) and $(Zn_{1+x}Ge)(N_2O_x)$ (Figure 7C) provides p−d repulsion,[17] thereby lifting the top of the valance band and narrowing the band gap. A comparison between the band gaps of $ZnGeN_2$ and $(Zn_{1+x}Ge)(N_2O_x)$ reveals that larger valance band dispersion resulting from the energy difference between O2p and N2p orbitals in $(Zn_{1+x}Ge)(N_2O_x)$ causes the band gap to narrow sufficiently to allow the absorption of visible light. From the UV−vis DR spectra shown in Figure 6, the band gap energy of the $(Zn_{1+x}Ge)(N_2O_x)$ powders decrease with nitridation time, that is, with increasing zinc concentration and decreasing oxygen concentration, indicating that the main factor determining the band gap is p−d repulsion between Zn3d and N2p +O2p electrons in the $(Zn_{1+x}Ge)(N_2O_x)$ solid solution.

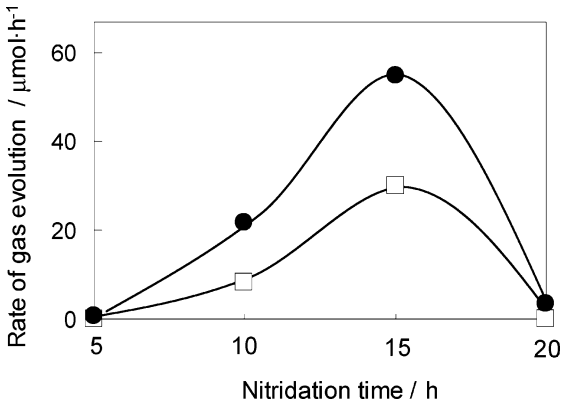

Figure 8. Dependence of photocatalytic activity of $(Zn_{1+x}Ge)(N_2O_x)$ under UV and visible irradiation (λ > 300 nm) on nitridation time. Circles denote H_2 evolution, squares denote O_2 evolution.

Dependence of Photocatalytic Activity on Nitridation Time. Figure 8 shows the dependence of the photocatalytic activity for overall water splitting on nitridation time for RuO_2 (5 wt %) loaded $(Zn_{1+x}Ge)(N_2O_x)$ powders under UV and visible irradiation (λ > 300 nm). The rates of H_2 and

(17) Wei, S. H.; Zunger, A. *Phys. Rev. B* **1988**, *37*, 8958.

Table 3. Photocatalytic Activities of Optimum (Zn$_{1+x}$Ge)(N$_2$O$_x$) Loaded with Various Cocatalysts under UV and Visible Irradiation (λ > 300 nm)

		photocatalytic activity (μmol h^{-1})[a]		
cocatalyst	wt %	H_2	O_2	N_2
none		0.1	n.d.	n.d.
RuO_2	5	54.3	27.5	n.d.
Cr_2O_3	0.5	0.1	n.d.	n.d.
Fe_2O_3	0.5	0.1	n.d.	n.d.
Co_3O_4	0.5	1.9	n.d.	n.d.
NiO	0.5	0.6	n.d.	n.d.
CuO	0.5	0.6	n.d.	n.d.
ZnO	0.5	0.5	n.d.	n.d.
Rh_2O_3	0.5	6.0	n.d.	n.d.
$Rh_{2-x}Cr_xO_3$	0.5(Rh)−0.2(Cr)	115.7	55.5	0.1
$Rh_{2-x}Cr_xO_3$	3.0(Rh)−0.2(Cr)	414.5	202.3	0.3

[a] n.d. = Not determined.

O_2 evolution increased with nitridation time to a maximum at 15 h with activities of 54.3 μmol h^{-1} (H_2) and 27.5 μmol h^{-1} (O_2), above which the activity of the sample began to decrease. Almost stoichiometric H_2 and O_2 evolution was achieved over RuO_2 (5 wt %) loaded (Zn$_{1+x}$Ge)(N$_2$O$_x$) powders nitrided for 10−15 h. A smaller ratio of H_2 to O_2 than the stoichiometric ratio, 2.0 is probably due to the photoreduction of O_2 to O_2^- during overall water splitting.[18,19] A small amount of H_2 was detected over the 5 h nitrided sample, but no evolution of O_2 was observed. The low photocatalytic activity of the 5 h nitrided sample is probably due to the poor crystallinity of the sample, which can be confirmed by the large half-widths of the XRD peaks and irregularly shaped particles with rough surfaces of the SEM image. Nitridation for longer than 15 h also had the effect of degrading the photocatalytic activity. Zinc in the compound can be easily volatized to Zn vapor during extended nitridation, resulting in defects in the 20 h nitrided sample, as confirmed by the UV−vis DR spectrum (Figure 6E). The decrease in activity for the 20 h nitrided (Zn$_{1+x}$Ge)(N$_2$O$_x$) sample is therefore considered to be associated with the increase in the number of defects, which act as recombination centers between photogenerated electrons and holes. These results indicate that the most suitable nitridation time for the preparation of (Zn$_{1+x}$Ge)(N$_2$O$_x$) solid solution as an active photocatalyst is 15 h under conditions of 1123 K and NH_3 flow rate of 20 mL min^{-1}. Under these conditions, optimum crystallinity is obtained through complete reaction between the starting materials without volatilization of zinc.

Effect of Cocatalyst on Photocatalytic Activity. Table 3 shows the photocatalytic activities of (Zn$_{1.44}$Ge)(N$_{2.08}$O$_{0.38}$) samples prepared with various cocatalysts under UV and visible irradiation (λ > 300 nm), where (Zn$_{1.44}$Ge)(N$_{2.08}$O$_{0.38}$) is the composition of the solid solution prepared under the optimum nitridation conditions of 1123 K for 15 h with NH_3 flow of 20 mL min^{-1}. (Zn$_{1.44}$Ge)(N$_{2.08}$O$_{0.38}$) alone exhibits little photocatalytic activity for water decomposition. Among the cocatalysts examined in the present study, Fe_2O_3, Co_3O_4, NiO, CuO, or ZnO was identified to be inactive. Rhodium oxide or chromium oxide alone also did not increase the photocatalytic activity, producing only a small amount of hydrogen. However, when loaded with a combination of rhodium and chromium oxides, a remarkable enhancement was achieved in photocatalytic activity. Modification of (Zn$_{1.44}$Ge)(N$_{2.08}$O$_{0.38}$) with 5 wt % RuO_2 afforded stoichiometric decomposition of water to H_2 and O_2 with activities of 54.3 μmol h^{-1} for H_2 and 27.5 μmol h^{-1} for O_2 (Figure 9A). However, when loaded with a $Rh_{2-x}Cr_xO_3$ mixed oxide consisting of 3.0 wt % Rh and 0.2 wt % Cr, the activity of (Zn$_{1.44}$Ge)(N$_{2.08}$O$_{0.38}$) increased to 414.5 μmol h^{-1} for H_2 evolution and 202.3 μmol h^{-1} for O_2 evolution (Figure 9B). This activity is 8 times higher than that for the 5 wt % RuO_2-modified sample, and 4000 times higher than for unmodified (Zn$_{1.44}$Ge)(N$_{2.08}$O$_{0.38}$) (Table 3). These results suggest that the photocatalytic performance of (Zn$_{1.44}$Ge)(N$_{2.08}$O$_{0.38}$) is strongly dependent on the kind and amount of cocatalyst, and that among the compositions examined in the present study, the optimum catalyst consists of (Zn$_{1.44}$Ge)(N$_{2.08}$O$_{0.38}$) loaded with $Rh_{2-x}Cr_xO_3$ (3.0 wt % Rh, 0.2 wt % Cr). However, the photocatalytic activity of $Rh_{2-x}Cr_xO_3$-loaded (Zn$_{1.44}$Ge)(N$_{2.08}$O$_{0.38}$) was gradually decreased with increasing reaction time under UV light irradiation (λ > 300 nm). The decrease in photocatalytic activity is attributed to the leaching of Zn and Cr from $Rh_{2-x}Cr_xO_3$-loaded (Zn$_{1.44}$Ge)(N$_{2.08}$O$_{0.38}$) catalyst confirmed by ICP measurements. No decrease in photocatalytic activity over 5 wt % RuO_2-modified sample suggests that the critical reason for decreasing activity on $Rh_{2-x}Cr_xO_3$-loaded (Zn$_{1.44}$Ge)(N$_{2.08}$O$_{0.38}$) is the instability of $Rh_{2-x}Cr_xO_3$ cocatalyst under UV light irradiation. (λ > 300 nm).

Photoreduction of H^+ to H_2 and photooxidation of H_2O to O_2 in the presence of a sacrificial electron donor (methanol) and acceptor (Ag^+) were examined under UV and visible irradiation (λ > 300 nm) in order to elucidate the role of the cocatalyst in the photocatalytic reaction for overall water splitting. The results are shown in Table 4. The results for photoreduction and photooxidation over

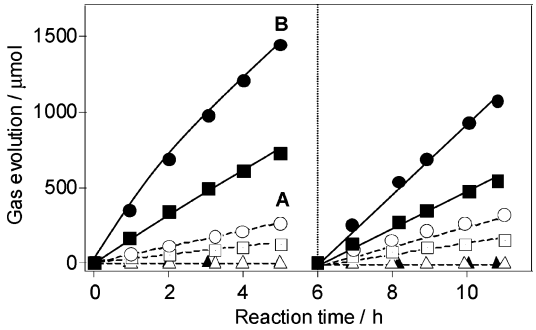

Figure 9. Time courses of gas evolution for optimum (Zn$_{1+x}$Ge)(N$_2$O$_x$) loaded with (A) 5 wt % RuO_2 and (B) $Rh_{2-x}Cr_xO_3$ (3.0 wt % Rh, 0.2 wt % Cr) under UV−visible light (λ > 300 nm). Circles denote H_2 evolution, squares denote O_2 evolution, and triangles denote N_2 production.

Table 4. Photoreduction and Photooxidation Activities of Optimum (Zn$_{1+x}$Ge)(N$_2$O$_x$) Loaded with Various Cocatalysts under UV−visible Light (λ > 300 nm)

cocatalyst	wt %	photoreduction (H_2 evolution) (μmol h^{-1})	photooxidation (O_2 evolution) (μmol h^{-1})
none		n.d.	46.3
RuO_2	5	2.4	57.9
$Rh_{2-x}Cr_xO_3$	3.0(Rh)−0.2(Cr)	153.4	38.3
Pt	1	13.3	44.2

(18) Domen, K.; Kudo, A.; Onishi, T. *J. Catal.* **1986**, *102*, 92.
(19) Maeda, K.; Teramura, K.; Masuda, H.; Takata, T.; Saito, N.; Inoue, Y.; Domen, K. *J. Phys. Chem. B* **2006**, *110*, 13107.

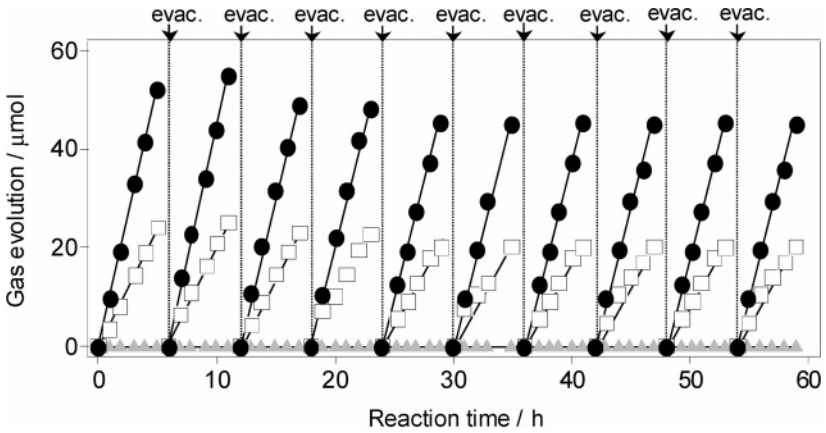

Figure 10. Time courses of gas evolution for optimum $(Zn_{1+x}Ge)(N_2O_x)$ loaded with $Rh_{2-x}Cr_xO_3$ (3.0 wt % Rh, 0.2 wt % Cr) under visible irradiation (λ > 420 nm). Circles denote H_2 evolution, squares denote O_2 evolution, and triangles denote N_2 production.

unmodified $(Zn_{1.44}Ge)(N_{2.08}O_{0.38})$ and Pt-modified $(Zn_{1.44}Ge)$-$(N_{2.08}O_{0.38})$ are also shown for comparison. $(Zn_{1.44}Ge)$-$(N_{2.08}O_{0.38})$ alone displayed no activity for hydrogen evolution even in the presence of an electron donor, yet afforded high activity for oxygen evolution (46 μmol h^{-1}). The high efficiency of photooxidation demonstrates that the photogenerated electrons and holes in the bulk are able to migrate to the surface. However, the low activity for H_2 evolution and high activity for O_2 evolution over unmodified $(Zn_{1.44}$-$Ge)(N_{2.08}O_{0.38})$ indicates the presence of surface states trapping photogenerated electrons, which are favorable for reducing Ag^+ ions but unfavorable for reducing H^+ to H_2. This tendency of high efficiency for photooxidation but low efficiency for photoreduction has also been observed for many oxynitride photocatalyst systems, including Ta_3N_5, TaON, $LaTiO_2N$, and $(Ga_{1-x}Zn_x)(N_{1-x}O_x)$, and is probably due to the presence of significant densities of defects in the bulk and surfaces of the materials.[20−23] These results suggest that the surface of unmodified $(Zn_{1.44}Ge)(N_{2.08}O_{0.38})$ hosts oxygen-evolution sites but not hydrogen-evolution sites.

Modification of $(Zn_{1.44}Ge)(N_{2.08}O_{0.38})$ with 5 wt % RuO_2 raised the H_2 evolution activity from zero to 2.4 μmol h^{-1}. The activity for O_2 evolution was also increased, even though the original oxygen-evolution sites on the catalyst surface had been covered with RuO_2. This result suggests that RuO_2 acts as not only a hydrogen-evolution site, but also an oxygen-evolution site. RuO_2 has been demonstrated by many researchers to be effective both as an oxidation site for the evolution of O_2 gas[24−26] and as a reduction site for H_2 evolution.[27−29] Kalyanasundaram et al. showed that colloidal RuO_2 provided highly effective mediation of the back conversion of $Ru(bpy)_3^{3+}$ to $Ru(bpy)_3^{2+}$ under the simultaneous production of oxygen.[24] Amouyal et al., on the other hand, revealed that RuO_2 enhances H_2 evolution in the presence of $Ru(bpy)_3^{2+}$, MV^{2+}, and EDTA.[27,28] Loading with RuO_2 therefore appears to improve both hydrogen- and oxygen-evolution sites for overall water splitting over $(Zn_{1.44}$-$Ge)(N_{2.08}O_{0.38})$. Loading with $Rh_{2-x}Cr_xO_3$ (3.0 wt % Rh, 0.2 wt % Cr) resulted in substantially enhanced H_2 evolution from methanol over $(Zn_{1.44}Ge)(N_{2.08}O_{0.38})$, with performance up to 60 times higher than achieved over the 5 wt % RuO_2-modified sample, and even 10 times higher than that for 1 wt % Pt-modified $(Zn_{1+x}Ge)(N_2O_x)$, which is known as a highly active reduction catalyst. In this case, however, the activity of O_2 evolution over $Rh_{2-x}Cr_xO_3$ (3.0 wt % Rh, 0.2 wt % Cr) modified $(Zn_{1.44}Ge)(N_{2.08}O_{0.38})$ was slightly depressed, attributable to the loss of oxygen-evolution sites. Maeda et al. reported stoichiometric evolution of H_2 and O_2 from distilled water under visible irradiation over $(Ga_{1-x}Zn_x)(N_{1-x}O_x)$ loaded with a mixed rhodium and chromium mixed, attributable to enhanced H_2 evolution.[3] The present results reveal that $Rh_{2-x}Cr_xO_3$ acts as a hydrogen-evolution site, and the increased activity for photocatalytic overall water splitting for the mixed-oxide-modified samples is primarily due to the improvement of hydrogen-evolution sites. RuO_2 or $Rh_{2-x}Cr_xO_3$ seems to have different effects on the migration of photoexcited electrons or holes from $(Zn_{1.44}Ge)(N_{2.08}O_{0.38})$ to each cocatalyst. Thus, investigation of the interlayer between $(Zn_{1.44}Ge)(N_{2.08}O_{0.38})$ and cocatalyst is important to understand the roles of cocatalyst. More details about the roles of each cocatalyst are still under investigation.

Figure 10 shows the time courses of H_2 and O_2 evolution over $Rh_{2-x}Cr_xO_3$ (3.0 wt % Rh, 0.2 wt % Cr)-loaded $(Zn_{1.44}$-$Ge)(N_{2.08}O_{0.38})$ under visible irradiation (λ > 420 nm). The photocatalytic performance of this system remained stable for more than 50 h of reaction, proceeding with stoichiometric H_2/O_2 production (within experimental error) and no N_2 evolution. The rate of H_2 and O_2 evolution in the second and subsequent runs with intermittent evacuation was also unchanged, and the reaction continued to proceed steadily

(20) Hitoki, G.; Ishikawa, A.; Takata, T.; Kondo, J. N.; Hara, M.; Domen, K. *Chem. Lett.* **2002**, 736−737.
(21) Hitoki, G.; Takata, T.; Kondo, J. N.; Hara, M.; Kobayashi, H.; Domen, K. *Chem. Commun.* **2002**, 1698−1699.
(22) Kasahara, A.; Nukumizu, K.; Hitoki, G.; Takata, T.; Kondo, J. N.; Hara, M.; Kobayashi, H.; Domen, K. *J. Phys. Chem. A* **2002**, *106*, 6750−6753.
(23) Maeda, K.; Teramura, K.; Masuda, H.; Takata, T.; Saito, N.; Inoue, Y.; Domen, K. *J. Phys. Chem. B* **2006**, *110*, 13107−13112.
(24) Kalyanasundaram, K.; Gratzel, M. *Angew. Chem., Int. Ed.* **1979**, *18*, 701.
(25) Kawai, T.; Sakata, T. *Nature (London*) **1980**, *286*, 474.
(26) Borgarello, E.; Kiwi, J.; Pelizzetti, E.; Visca, M.; Gratzel, M. *Nature (London*) **1981**, *289*, 158.
(27) Amouyal, E.; Keller, P.; Moradpour, A. *J. Chem. Soc., Chem. Commun.* **1980**, 1019.
(28) Keller, P.; Moradpour, A.; Amouyal, E. *J. Chem. Soc., Faraday Trans. 1* **1982**, *78*, 3331.
(29) Sakata, T.; Hashimoto, K.; Kawai, T. *J. Phys. Chem.* **1984**, *88*, 5214.

with activities of 11.1 μmol h^{-1} for H_2 and 5.4 μmol h^{-1} for O_2. The total amount of H_2 and O_2 evolved over 50 h under visible irradiation was 0.76 mmol, greater than the amount of catalyst employed (0.10 g, 0.50 mmol of $(Zn_{1.44}Ge)(N_{2.08}O_{0.38})$). No changes in the XRD patterns and no leaching of any metals, including Ge, Zn, Rh, and Cr, could be detected by XRD or ICP-OES measurement following the photocatalytic reactions. The quantum efficiency for overall water splitting activity at 420 nm is estimated to be ca. 0.20%. These results show that surface modification of $(Zn_{1.44}Ge)(N_{2.08}O_{0.38})$ by impregnation of $Rh_{2-x}Cr_xO_3$ as a cocatalyst results in a stable and effective photocatalyst for overall water decomposition under visible irradiation. Further enhancement in photocatalytic activity for overall water splitting is expected through improvement of hydrogen- and oxygen-evolution sites.

Conclusions

Zinc germanium oxynitride, $(Zn_{1+x}Ge)(N_2O_x)$, a solid solution between ZnO and $ZnGeN_2$, was prepared by nitridation of GeO_2 and ZnO under a NH_3 flow of 20 mL min^{-1} at 1123 K. The change in the product with nitridation time was examined, and it was revealed that the solid-solution phase forms after just 5 h of nitridation, with further nitridation proceeding until the reaction between $(Zn_{1+x}Ge)(N_2O_x)$ and ZnO has consumed all the starting materials after approximately 15 h. Further nitridation caused volatilization of zinc in $(Zn_{1+x}Ge)(N_2O_x)$, resulting in symmetry change from wurtzite to an orthorhombic structure. The nitrogen and zinc contents in $(Zn_{1+x}Ge)(N_2O_x)$ increased with nitridation time from 5 to 15 h, whereas the oxygen content decreased. The 5−15 h nitrided samples exhibited a single phase of wurtzitic $(Zn_{1+x}Ge)(N_2O_x)$, which was found to be responsive to visible light with a band gap of ca. 2.7−2.8 eV. The band gap decreased marginally with increasing nitridation time, that is, with increasing zinc content. This narrowing of the band gap is attributable to p−d repulsion between Zn3d and N2p+O2p electrons in the upper valance band, which raises the top of the valance band. The optimum preparation conditions for $(Zn_{1+x}Ge)(N_2O_x)$ in order to achieve high photocatalytic activity for overall water splitting are thus considered to be 15 h nitridation at 1123 K under NH_3 flow at 20 mL min^{-1}. The catalyst produced under these conditions has high crystallinity, achieved by complete reaction between starting materials without volatilization of zinc. Among the range of cocatalysts examined, a mixed oxide of $Rh_{2-x}Cr_xO_3$ was found to be the most effective for enhancing the photocatalytic activity of $(Zn_{1+x}Ge)(N_2O_x)$, primarily through the production of highly effective hydrogen-evolution sites. The optimally nitrided catalyst with composition $(Zn_{1.44}Ge)(N_{2.08}O_{0.38})$, loaded with $Rh_{2-x}Cr_xO_3$ (3.0 wt % Rh, 0.2 wt % Cr), provides photocatalytic overall water decomposition under visible irradiation with quantum efficiency of ca. 0.20% at 420 nm.

Acknowledgment. The authors gratefully acknowledge the assistance of Dr. T. Ashino of the Analytic Research Core for Advanced Materials, Institute for Materials Research, Tohoku University, for elemental analyses. This work was supported by the Solution Oriented Research for Science and Technology (SORST) program of the Japan Science and Technology Corporation (JST).

CM062980D